Optica Applicata, Vol. LI, No. 1, 2021
DOI: 10.37190/oa210106

Broadband fluorescence emission and laser demonstration in large mode waveguide structure in Yb^{3+} doped germanate glass

MAMOONA KHALID

School of Engineering, University of South Australia;
khamy062@mymail.unisa.edu.au

A stable composition (against crystallization) of germanate glass doped with Yb^{3+} for mid-infrared laser applications is presented. Broad emission spectrum of Yb^{3+} was obtained for the fabricated glass. Laser operation was demonstrated in 13 mm long waveguide written in the glass using a femtosecond laser operating at 524 nm center wavelength sending 250 fs ultrashort pulses. The resulting CW laser operated at 1.04 μm in the fundamental mode of the waveguide. The propagation loss through the waveguide was 0.6 dB/cm at 1550 nm for 45 μm diameter of the modified structure. The mode analysis of the developed waveguide structure is also presented in COMSOL Multiphysics to study the electric field distribution through different modes of propagation in the waveguide and the confinement loss associated to them.

Keywords: germanate glass, ultrafast waveguide writing, near-infrared laser operation, high linear and nonlinear refractive index.

1. Introduction

New laser materials in the near- and mid-infrared region are in high demand these days for a number of applications including absorption spectroscopy; remote sensing based on LIDAR; optical signal processing; free space optical communication; atmospheric monitoring; biomedical sensing; micromachining; medical surgery; pharmaceutical industry for product sanitization; military and a number of defense related applications [1]. In the recent years the germanate glass has been the focus of research for laser and nonlinear applications in mid-infrared region as it comprises numerous valuable properties such as its higher glass transition temperature, high density, elevated linear and nonlinear refractive index and thermal, chemical and mechanical stability when compared to other soft glasses.

Previously silicates and fluorides have widely been researched as the host material for laser applications. Silicates have high damage threshold values and are thermally stable, yet they have limited transmission characteristics in a mid-infrared range. Flu-

orides on the other hand have wider transmittance spectrum in mid-infrared region, however they have low thermal, chemical and mechanical stability compared to heavy metal oxide glasses [2, 3]. Germanate, a member of heavy metal oxide glasses, on the other hand has shown broader infrared transmission ($\lambda \leq 7$–10 μm) and is considered to be a good host material due to its greater chemical durability and mechanical strength [4]. Its phonon energy, responsible for non-radiative decay leading towards thermal load on the glass, is less than silicates. It also has a strong capability to accommodate large concentrations of dopants like in fluorides, however with improved thermal, chemical and mechanical stability [5].

In this study, a new Yb^{3+} doped germanate glass with broad emission spectrum in the near- to mid-infrared region was fabricated. This study was commenced to understand the interaction of active laser ions with the host ligand, femtosecond laser interaction for waveguide fabrication and the suitability of host material for 2 μm waveguide laser development in Yb^{3+}/Ho^{3+} co-doped germanate glass having the same composition being the main motivation of the current work. Although a spectroscopic analysis of 2 μm germanate based glass doped with Tm^{3+} [6], Yb^{3+}/Ho^{3+} [5, 7–12], Tm^{3+}/Ho^{3+} [6], $Er^{3+}/Tm^{3+}/Ho^{3+}$ [13] reported earlier has shown its capability for laser application in mid-infrared region, yet only a few studies were reported on the development of waveguide lasers with waveguides inscribed in these glasses using the emerging ultrafast laser inscription (ULI) technique. This limitation is probably due to the difficulty in achieving controlled nonlinear waveguide structure in germanate because of its small band gap ($E_g \approx 2$–3 eV) and its high linear ($n_0 \sim 1.85$) and nonlinear refractive index ($n_2 \sim 5.6 \pm 6 \times 10^{-20}$ m^2/W) [2]. Large n_2 values may lead to strong self-focusing even at lower optical power producing spatial energy distribution that becomes difficult to be controlled forming non-circular and thus lossy waveguides [2].

2. Yb^{3+}: GPGN spectroscopic analysis

A new germanate glass sample GPGN with composition GeO_2-PbO-Na_2O-Ga_2O_3 doped with 3 mol% Yb^{3+} was fabricated in dry glove box environment. The 20 g batch was melted in a platinum crucible at 1250°C for about 2 hours. The cast was then annealed at about 390°C in a brass mould followed by post annealing process for about 15 hours to reduce thermal stress in the sample. The resulting glass had dimensions of $30 \times 15 \times 4$ mm^3 and was optically polished before taking the fluorescence measurements using spectrofluorimeter (Edinburgh Instruments FLS980).

The fluorescence in Yb^{3+} is a simple and straightforward process as it has only two energy levels, the ground state $^2F_{7/2}$ and the excited energy level $^2F_{5/2}$. The emission spectrum obtained for the fabricated germanate glass was observed to be broader compared to that in other glass hosts. To confirm this, the emission spectrum in the fabricated sample was compared to the well-known fluoride glass (ZBLAN), having the same Yb^{3+} concentration (Fig. 1) under the same conditions at room temperature. The samples were excited using 976 nm laser diode. Broader fluorescence for GPGN along with

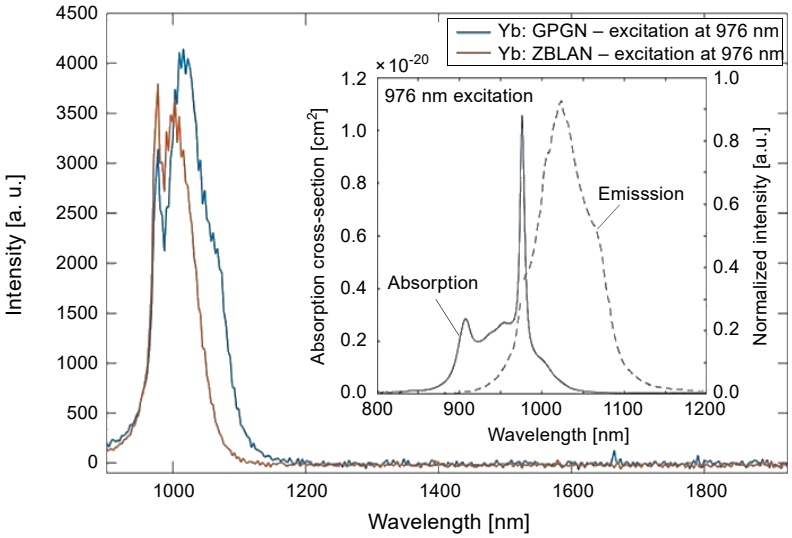

Fig. 1. Comparison of emission profile of Yb^{3+} in GPGN (broader emission) and ZBLAN (red). Inset shows the absorption and normalized emission cross-sections of Yb^{3+} in fabricated GPGN.

a blue shifted emission peak above 980 nm was observed. The 976/980 nm emission peak of Yb^{3+} ($^2F_{7/2}$), however, is irrespective of the host material and is observed in all glass types (silicates, fluorides, phosphates, chalcogenides and heavy metal oxide glasses). This red shifted peak in GPGN and broader emission spectrum (950–1150 nm) is attributed to larger stark splitting in germanate glass compared to other host materials [14]. It is believed that larger stark splitting makes the Yb^{3+} doped laser in a glass material to function closer to quasi-four level system rather than quasi-three level and thus has the potential of improving the laser efficiency [2]. In order to achieve higher laser efficiency, YANG *et al*. [15] recommended to accomplish larger stark splitting for Yb^{3+} instead of improving the absorption and emission cross-sections which in case of germanate and silicate is making GPGN a better host material for infrared applications compared to other glasses [6, 16]. Inset in Fig. 1 represents the emission and absorption cross-sections for the fabricated germanate glass.

3. Waveguide writing

To present the potential of the fabricated GPGN glass to be utilized for fiber laser application in the mid-infrared region, its laser capability for small scale waveguide laser in Yb^{3+} doped GPGN sample was first analyzed. For this purpose, single line waveguides were inscribed in the fabricated germanate glass using frequency doubled femtosecond laser (IMRA FCPA μ-Jewel) with center wavelength 524 nm having pulse duration of 250 fs. The waveguides were written in cumulative thermal regime [3, 17] using 5 MHz repetition rate (RR). The ultrafast laser pulse energy ranged from 15 to 80 nJ. By in-

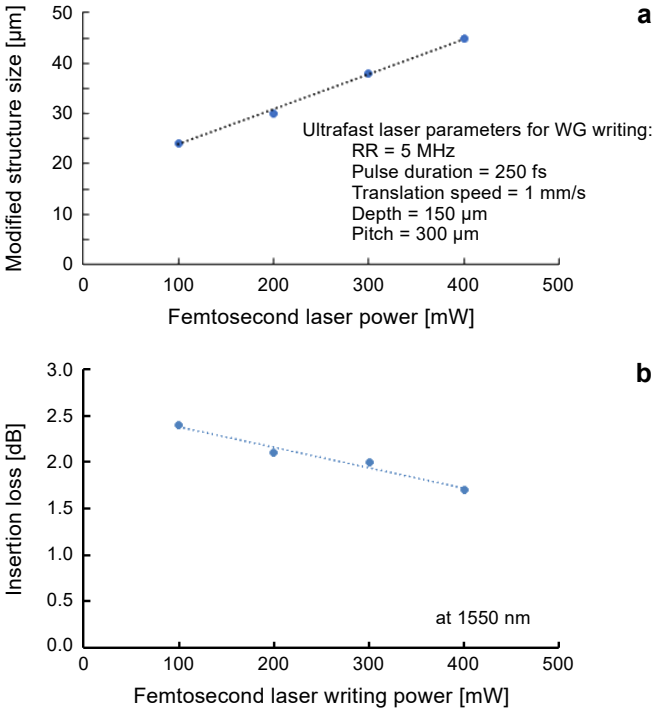

Fig. 2. Increasing trend in waveguide size by increasing ultrafast laser pulse energy (**a**). Insertion loss in written waveguides (**b**).

creasing the pulse energy of ultrafast laser, the structural modification and hence the size of the guiding waveguide increased as observed in Fig. 2**a**. The waveguide loss measured at 1550 nm decreased by increasing the pulse energy. The highest loss of 2.4 dB was observed for the waveguide written with 20 nJ while for 80 nJ the loss reduced to 1.7 dB (Fig. 2**b**). The diameter of the modified structure with 80 nJ was $D = 45$ μm with central confined mode of ~24 μm which supported the laser operation.

For waveguide writing the sample was placed on an air bearing *x*-*y*-*z* stage (Aerotech ABL9000) and was translated with speed of 1 mm/s. ZEISS 100× oil immersive objective having NA = 1.25 was utilized to focus down the ultrafast laser pulses 50 μm and 150 μm underneath the surface of the sample to find the optimum writing depth. The resulting waveguides were multimode in nature having bright tear drop structure with positive refractive index change in the vicinity of the focal volume (Fig. 3). By increasing the pulse energy, the central core started to appear at 20 nJ which became brighter at higher pulse energies with reduction in waveguide loss (Fig. 2**b**). No laser operation was observed below 20 nJ of laser pulse energy due to the absence of central core (mode) although the brighter modified structure (higher order modes) was still present surrounding the focal volume. It was observed that the waveguides that were written 50 μm down the surface of the sample cracked for these pulse energies. As we go deeper

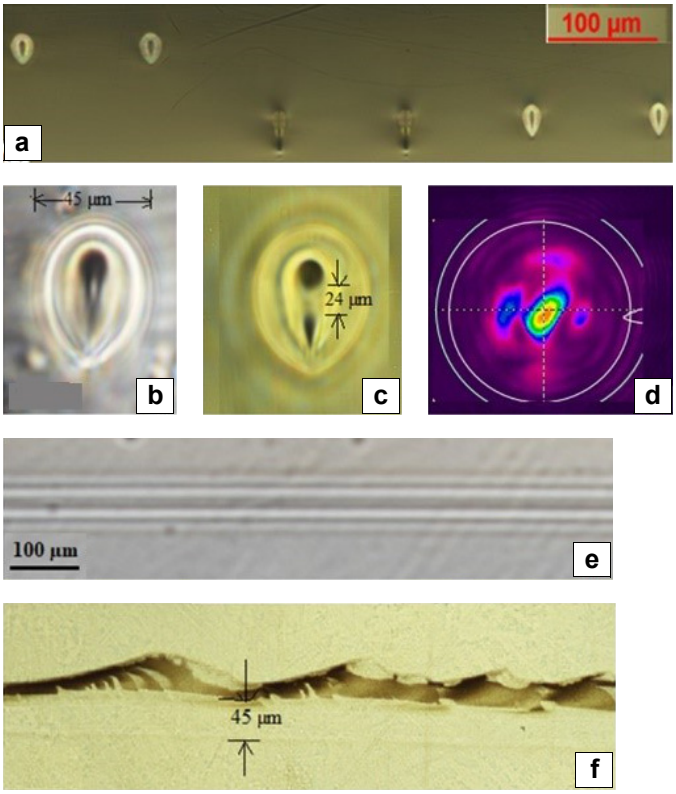

Fig. 3. Written waveguides at 50 and 150 µm depth (**a**). Similar scale microscopic images of modified structure in GPGN written with 400 mW (**b**, **c**). Beam propagation through 24 µm mode for loss measurement (**d**). Lateral view of inscribed waveguide 150 µm underneath the surface (**e**). Lateral view of cracked waveguide 50 µm underneath the surface due to thermal stress (**f**).

into the sample, the ellipticity of the waveguides increased due to the spherical aberration introduced because of refractive index mismatch between the sample (1.85) and the oil immersion objective (1.5). The structure produced by femtosecond laser had different refractive index distribution within the modified area giving multiple modes of beam propagation (bright region) as shown in Figs. 3**b** and 3**c** with the central mode (core) more confined compared to surrounding bright structures. Beam propagation through the central mode $D = 24$ µm is shown in Fig. 3**d**. Figures 3**e** and 3**f** represents the lateral views of 150 and 50 µm (cracked) modified structures, respectively.

4. Mode analysis and confinement loss

The cross-sectional waveguide structure was modelled in COMSOL Multiphysics to study different modes propagating through the waveguide and to find the confinement loss for each mode propagating in the modified structure. COMSOL is a powerful tool

that uses the finite element method for mesh formation and mode analysis. The 2D mode analysis with electromagnetic frequency domain within the wave optic module was selected for this purpose. The geometry for the waveguide structure was defined according to the 5 MHz RR cross-sectional structure obtained from femtosecond laser inscription. The material was defined according to its respective core and cladding refractive indices with the refractive index of the core slightly greater than that of cladding, with $n_{core} = 1.85144$ and $n_{cladding} = 1.85$. The 3µm thick perfectly matched layer (PML) as boundary condition was selected to avoid any scattering or electric field reflecting from the boundary to calculate the confinement loss in the fundamental mode and higher order modes. The mesh elements were selected to be finer for the accuracy in the analysis.

Figure 4 represents the mesh formation for the waveguide and the power flow in the direction of propagation (*z* direction) for the fundamental mode with effective mode index ~1.8506. Table 1 gives the evaluation of global parameters for the fundamental mode and higher order modes for this specific structure with highlighted mode as the fundamental mode with the maximum power flow in *z* direction. Electric field in *z* direction for fundamental mode and higher order modes is given in Fig. 5.

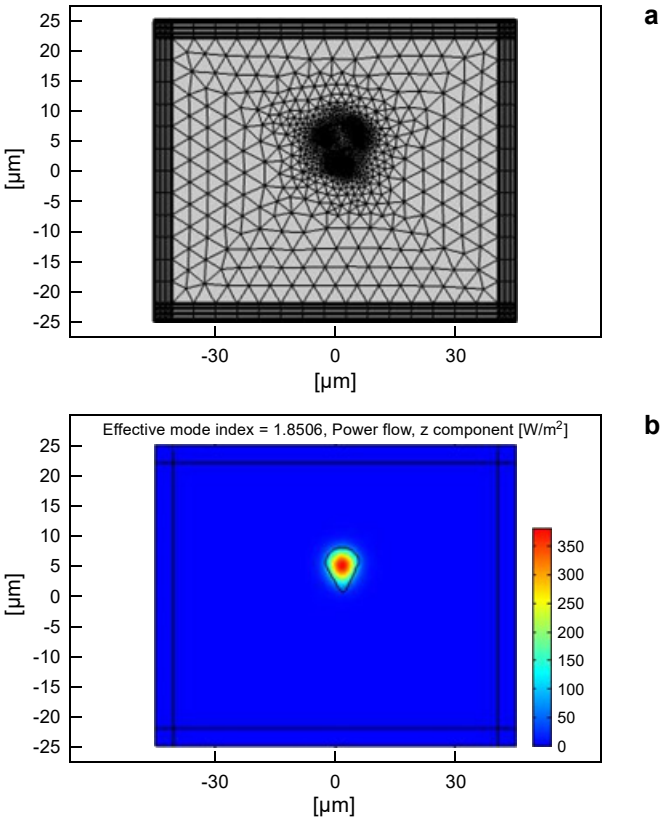

Fig. 4. Finer mesh formation for the waveguide structure in COMSOL with 3 µm layer of PML (**a**). Beam propagation through the waveguide core in *z* direction (**b**).

T a b l e 1. Mode parameters for different modes of propagation of the designed waveguide.

Effective mode index at 1550 nm	Propagation constant at 1550 nm [rad/m]	Attenuation constant at 1550 nm [rad/m]	Attenuation constant at 976 nm [rad/m]
1.8506	7.5×10^6	1.1476	–0.0020603
1.8506	**7.5×10^6**	**1.1512**	**0.0020236**
1.85	7.5×10^6	3.6165	26.082
1.85	7.5×10^6	3.6236	46.714
1.85	7.5×10^6	3.7086	52.24
1.85	7.5×10^6	3.7207	58.696

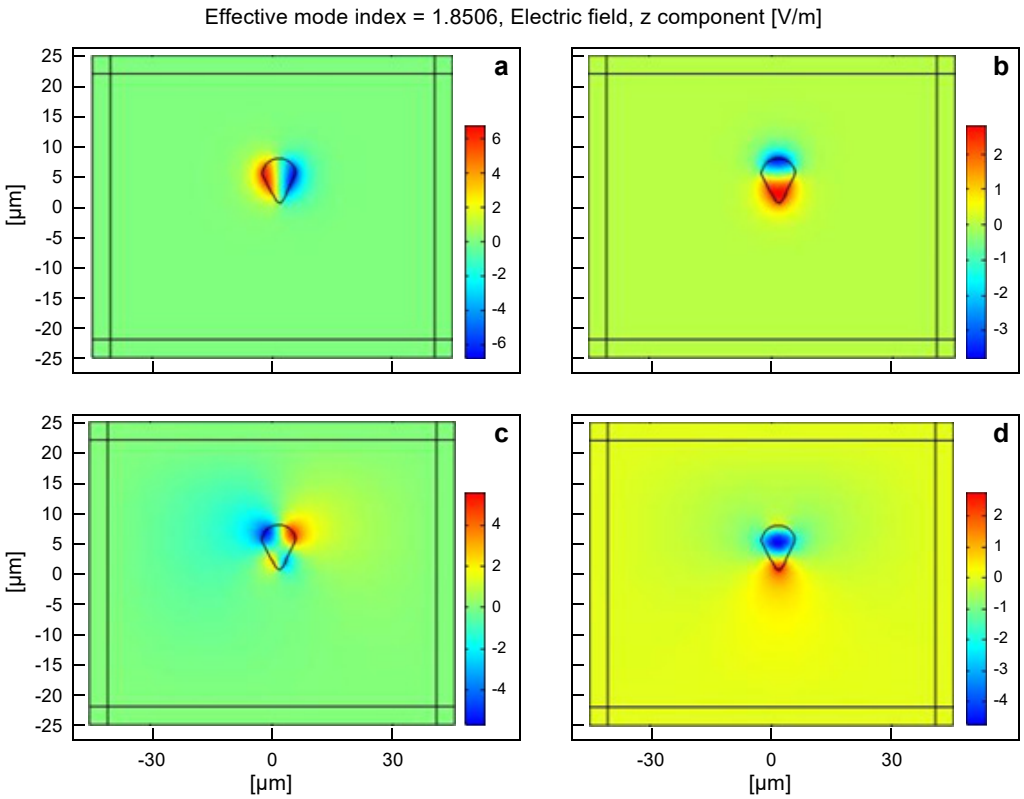

Fig. 5. Electric field z component distribution in fundamental (**a**) and higher order (**b**–**d**) modes of propagation within the elliptically designed waveguide structure.

The power flow decays with an attenuation factor of γ as it propagates through the waveguide. In order to calculate the loss in the waveguide, the evaluation of γ in the j-th mode is required. To obtain γ, the excitation electromagnetic power in the j-th mode at excitation frequency can be expressed as [18]

$$P_{E_j}(z) = \left|a_{E_j}\right|^2 N_{E_j} \exp(-\gamma_{E_j} z) \tag{1}$$

$$N_{E_j} = \frac{1}{2}\mathrm{Re}\left\{\int (\mathbf{e}_{E_j} \times \mathbf{h}_{E_j}) \cdot \hat{\mathbf{z}}\,\mathrm{d}A\right\} \tag{2}$$

$$\gamma_{E_j} = k\left(\frac{\varepsilon_0}{\mu_0}\right)^{1/2} \frac{1}{N_{E_j}} \int n_{E_j} n_{E_j}^{\mathrm{i}} \left|e_{E_j}\right|^2 \mathrm{d}A \tag{3}$$

where a_{Ej} is the expansion coefficient in j-th mode, $\mathbf{e}_{Ej}(x, y)$, $\mathbf{h}_{Ej}(x, y)$, and γ_{Ej} are the j-th mode electric and magnetic field distributions and the power delay factor. ε_0 is the permittivity of free space (8.854×10^{-12} $\mathrm{m^{-3} \cdot kg^{-1} \cdot s^4 \cdot A^2}$) and μ_0 is the free space permeability (1.26×10^{-6} $\mathrm{m \cdot kg \cdot s^{-2} \cdot A^{-2}}$). Only fundamental mode is considered here for the final calculation of γ_{Ej} as its confinement loss is lower compared to higher order modes. The integration parameters given in Eqs. (1)–(3) are evaluated for the current waveguide structure and are presented in Table 2. The real n_{E_j} and imaginary $n_{E_j}^{\mathrm{i}}$ part of effective refractive index are constants. The imaginary part of refractive index was determined from the attenuation constant of the respective fundamental mode and was measured to be ~2.84×10^{-7} using the equation $\alpha = k\,\mathrm{Im}(n_{\mathrm{eff}})$ where $k = 2\pi/\lambda$ with λ being the wavelength. The value of $\lambda = 1550$ nm was utilized for the simulation purpose. The power delay factor of the fundamental mode was calculated to be 0.637 dB/cm (0.828 dB for 1.3 cm long waveguide). The low attenuation constant as given in Table 2 for 1550 and 976 nm in the fundamental mode (central core of modified structure) represents better wave confinement and shows that only this mode can take part in laser operation while the higher order modes tend to leak into the cladding due to a very small refractive index change. For the excitation wavelength 976 nm, it can be observed from Table 2 that the attenuation constant for higher order modes is higher compared to the fundamental mode representing more confined central mode. The experimental insertion loss in the laser cavity mode was measured to be ~1.7 dB where 0.77 dB is the Fresnel loss due to high refractive index of the fabricated glass. If we consider the simulated propagation loss of 0.828 dB to be in close approximation to the experimental loss, the coupling loss will then be ~0.102 dB which matches the expected experimental value as there was a significant mismatch between the numerical aperture of

T a b l e 2. Power delay factor parameters for different modes of propagation in waveguide for 1550 nm simulation.

Effective mode index	$\int \left\|e_{Ej}\right\|^2$ (core) [$\mathrm{kg^2m^3s^{-6}A^{-2}}$]	$\int (\mathbf{e}_{Ej} \times \mathbf{h}_{Ej}) \cdot \hat{\mathbf{z}}\,\mathrm{d}A$ [$\mathrm{kg^2m^4s^{-4}}$]	$\int \left\|e_{Ej}\right\|^2$ (cladding) [$\mathrm{kg^2m^3s^{-6}A^{-2}}$]
1.8506	0.24856	$-9.5414 \times 10^{-10} - 5.7511 \times 10^{-13}i$	1.84×10^{-7}
1.8506	**0.71961**	$\mathbf{2.4881 \times 10^{-9} + 1.7110 \times 10^{-12}i}$	$\mathbf{1.81 \times 10^{-8}}$
1.85	0.66352	$-1.1029 \times 10^{-8} + 5.0998 \times 10^{-10}i$	4.8066
1.85	7.11×10^{-1}	$2.1518 \times 10^{-8} - 1.0673 \times 10^{-10}i$	12.194
1.85	2.01×10^{-1}	$-3.6314 \times 10^{-8} - 2.1092 \times 10^{-10}i$	12.556
1.85	2.07×10^{-1}	$-2.8495 \times 10^{-9} + 1.8549 \times 10^{-10}i$	2.1295

the focusing lens and the waveguide during the experiment. This confirms that the simulated propagation loss is in close approximation to the experimental value with only the fundamental mode being more confined for laser operation in contrast to the higher order modes.

5. 1041 nm laser operation in the waveguide

In this section we present the laser operation in the waveguide written in Yb^{3+}: GPGN using 80 nJ pulse energy and 5 MHz pulse repetition rate, 150 µm underneath the surface of the sample. It was observed that as the pulse energy was increased so does the mode size of the fundamental mode making it more confined to support the laser operation.

The 900 mW, 8 µm single mode 976 nm laser diode was utilized to pump the Yb^{3+} ions in the germanate sample using the setup discussed in our previous work [19]. The 1.5 mm collimated beam was passed through f = 26 mm focusing lens to focus it down to ~20 µm to match the mode size of the waveguide. The >95% T input coupler at 976 nm and 90% R output coupler at ~1 µm were butted up to the end facets of the waveguide giving the length of cavity L = 13 mm.

Figure 6 gives the laser operating at 1041 nm for 13 mm laser cavity. Slope efficiency of ~13% with ~32 mW output power at 750 mW input was achieved for the written waveguide in GPGN with a lasing threshold of ~350 mW. It was observed that the wavelength of the laser was red shifted compared to our previous work where it

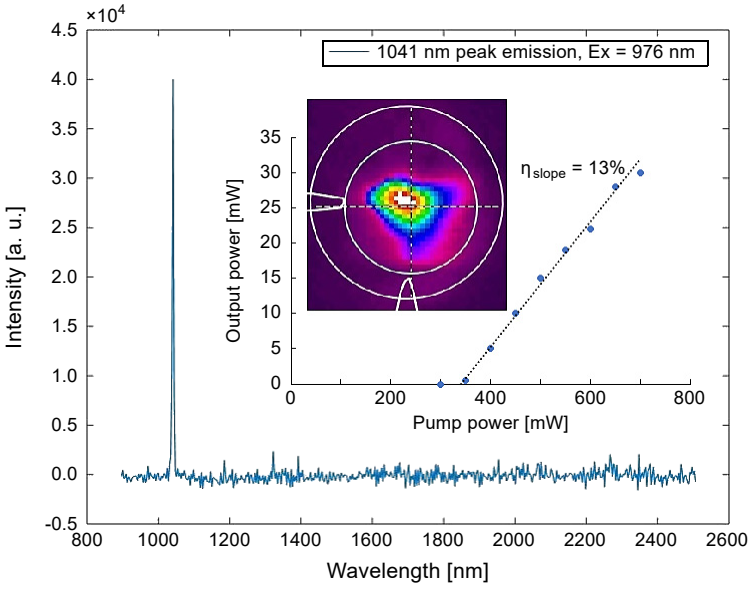

Fig. 6. Peak laser operation at 1041 nm for 24 µm waveguide core diameter. Inset to the figure is the output laser power achieved with 13% slope efficiency. Laser mode out of the waveguide is also shown in the inset.

operated at 1069–1075 nm for the same 13 mm long cavity. However, the laser efficiency was only 5% due to higher waveguide and coupling losses. This confirms that the broad emission gain for germanate glass can be achieved from ~950 to 1100 nm depending on the length and mode size of the laser cavity. We further are investigating the waveguide writing parameters in different writing regimes (thermal and athermal) to reduce the waveguide losses and further improve the laser efficiency before the waveguide laser demonstration in Yb^{3+}/Ho^{3+}: GPGN.

6. Conclusion

A new germanate GPGN glass comprising a thermally stable composition (against crystallization) of GeO_2-PbO-Ga_2O_3-Na_2O for mid-infrared fiber and waveguide laser applications has been fabricated and presented. Broadband emission with blue shifted emission peak compared to other host glasses was achieved for the fabricated sample because of larger stark splitting in germanate glass after silica. Waveguides were inscribed in the sample in the thermal regime (5 MHz) of femtosecond laser with laser pulse energy ranging from 15 to 80 nJ. Due to the interaction of femtosecond laser pulses with the host material with increasing pulse energy, an increase in the size of the modified structure was observed with a well confined core at higher pulse energy. Waveguide insertion loss was determined to be 1.7 dB at 1550 nm. This high loss was due to the spherical aberration induced into the sample due to a mismatch of refractive indices between the sample and the oil immersion objective that was designed for waveguide writing in lower refractive index glasses. Waveguide laser was demonstrated in the waveguide written with 80 nJ pulse energy as the core was more confined compared to other waveguides written with lower pulse energies. The laser operated at 1041 nm with 13% slope efficiency and is ~3 times greater than that achieved in our previous work for a small mode size. The laser threshold observed was 350 mW due to a large mode area of the waveguide. This laser efficiency can further be improved by reducing the spherical aberrations in the sample during the writing process along with improving the waveguide writing parameters for inscribing well defined circular structures.

Acknowledgment – This work was supported by AOARD project number FA2386-16-1-4068 conducted in University of South Australia.

References

[1] SEDDON A.B., TANG Z., FURNISS D., SUJECKI S., BENSON T.M., *Progress in rare-earth-doped mid-infrared fiber lasers*, Optics Express **18**(25), 2010, pp. 26704–26719, DOI: 10.1364/OE.18.026704.

[2] SIEGEL J., FERNÁNDEZ-NAVARRO J.M., GARCÍA-NAVARRO A., DIEZ-BLANCO V., SANZ O., SOLIS J., VEGA F., ARMENGOL J., *Waveguide structures in heavy metal oxide glass written with femtosecond laser pulses above the critical self-focusing threshold*, Applied Physics Letters **86**(12), 2005, article 121109, DOI: 10.1063/1.1888032.

[3] JIANG X., LOUSTEAU J., RICHARDS B., JHA A., *Investigation on germanium oxide-based glasses for infrared optical fibre development*, Optical Materials **31**(11), 2009, pp. 1701–1706, DOI: 10.1016/j.optmat.2009.04.011.

[4] FAN X., KUAN P., LI K., ZHANG L., LI D., HU L., *Spectroscopic properties and quenching mechanism of 2 μm emission in Ho^{3+} doped germanate glasses and fibers*, Optical Materials Express **5**(6), 2015, pp. 1356–1365, DOI: 10.1364/OME.5.001356.

[5] XU R., PAN J., HU L., ZHANG J., *2.0 μm emission properties and energy transfer processes of Yb^{3+}/Ho^{3+} codoped germanate glass*, Journal of Applied Physics **108**(4), 2010, article 043522, DOI: 10.1063/1.3468726.

[6] LIN Q., XIA H., ZHANG Y., WANG J., ZHANG J., HE S., *Gain properties of germanate glasses singly doped with Tm^{3+} and Ho^{3+} ions*, Journal of Rare Earths **27**(1), 2009, pp. 76–82, DOI: 10.1016/S1002-0721(08)60195-7.

[7] RAGIN T., BARANOWSKA A., KOCHANOWICZ M., ZMOJDA J., MILUSKI P., DOROSZ D., *Study of mid-infrared emission and structural properties of heavy metal oxide glass and optical fibre co-doped with Ho^{3+}/Yb^{3+} ions*, Materials **12**(8), 2019, article 1238, DOI: 10.3390/ma12081238.

[8] WEBER M., MATSINGER B.H., DONLAN V.L., SURRATT G.T., *Optical transition probabilities for trivalent holmium in LaF_3 and $YAlO_3$*, The Journal of Chemical Physics **57**(1), 1972, pp. 562–567, DOI: 10.1063/1.1678000.

[9] CAI M., ZHOU B., WANG F., TIAN Y., ZHOU J., XU S., ZHANG J., *Highly efficient mid-infrared 2 μm emission in Ho^{3+}/Yb^{3+}-codoped germanate glass*, Optical Materials Express **5**(6), 2015, pp. 1431–1439, DOI: 10.1364/OME.5.001431.

[10] BALAJI S., SONTAKKE A.D., SEN R., KALYANDURG A., *Efficient ~2.0 μm emission from Ho^{3+} doped tellurite glass sensitized by Yb^{3+} ions: Judd–Ofelt analysis and energy transfer mechanism*, Optical Materials Express **1**(2), 2011, pp. 138–150, DOI: 10.1364/OME.1.000138.

[11] KIR'YANOV A.V., BARMENKOV Y.O., MINKOVICH V.P., ANDRES M.V., *Nonlinear transmission coefficient of ytterbium-holmium fiber at the wavelength 978 nm*, Modern Trends in Laser Physics **17**(2), 2007, pp. 71–79, DOI: 10.1134/S1054660X07020041.

[12] KHALID M., LANCASTER D.G., EBENDORFF-HEIDEPRIEM H., *Spectroscopic analysis and laser simulations of Yb^{3+}/Ho^{3+} co-doped lead-germanate glass*, Optical Materials Express **10**(11), 2020, pp. 2819–2833, DOI: 10.1364/OME.404375.

[13] HUANG F., LIU X., LI W., HU L., CHEN D., *Energy transfer mechanism in Er^{3+} doped fluoride glass sensitized by Tm^{3+} or Ho^{3+} for 2.7μm emission*, Chinese Optics Letters **12**(5), 2014, article 051601.

[14] KUAN P.-W., FAN X., LI X., LI D., LI K., ZHANG L., YU C., HU L., *High-power 2.04 μm laser in an ultra-compact Ho-doped lead germanate fiber*, Optics Letters **41**(13), 2016, pp. 2899–2902, DOI: 10.1364/OL.41.002899.

[15] YANG B., LIU X., WANG X., ZHANG J., HU L., ZHANG L., *Compositional dependence of room-temperature Stark splitting of Yb^{3+} in several popular glass systems*, Optics Letters **39**(7), 2014, pp. 1772–1774, DOI: 10.1364/OL.39.001772.

[16] EL-RABAIE S., TAHA T.A., HIGAZY A.A., *Compositional dependence thermal and optical properties of a novel germanate glass*, Physica B: Condensed Matter **432**, 2014, pp. 40–44, DOI: 10.1016/j.physb.2013.09.020.

[17] GAN F., *Optical and Spectroscopic Properties of Glasses 245*, Shanghai Science and Technology Press, 1992.

[18] SHAHRAAM AFSHAR V., WARREN-SMITH S.C., MONRO T.M., *Enhancement of fluorescence-based sensing using microstructured optical fibres*, Optics Express **15**(26), 2007, pp. 17891–17901, DOI: 10.1364/OE.15.017891.

[19] KHALID M., CHEN G.Y., BEI J., EBENDORFF-HEIDEPRIEM H., LANCASTER D.G., *Microchip and ultra-fast laser inscribed waveguide lasers in Yb^{3+} germanate glass*, Optical Materials Express **9**(8), 2019, pp. 3557–3564, DOI: 10.1364/OME.9.003557.

Received January 29, 2020